ACTA METALLURGICA SLOVACA
2021, VOL. 27, NO. 4, 172-179

RESEARCH PAPER

PHYSICO-TRIBOLOGICAL CHARACTERISTICS AND WEAR MECHANISM OF HYBRID REINFORCED Al6063 MATRIX COMPOSITES

Peter Ikubanni[1], Makanjuola Oki[1], Adekunle Adeleke[1], Olanrewaju Adesina[1], Peter Omoniyi[2,3]*

[1] Department of Mechanical Engineering, Landmark University, Omu-Aran, Nigeria
[2] Department of Mechanical Engineering Science, University of Johannesburg, Johannesburg, South Africa
[3] Department of Mechanical Engineering, University of Ilorin, Ilorin, Nigeria

*Corresponding author: ikubanni.peter@lmu.edu.ng, tel.:+234-706-599-3936, Department of Mechanical Engineering, Landmark University, 251101, Omu-Aran, Kwara State

Received: 04.08.2021
Accepted: 14.10.2021

ABSTRACT

The development of engineering materials is continuously attracting attention from scientists and engineers for numerous engineering applications. The physical properties and wear mechanism of aluminium (Al 6063) matrix reinforced with silicon carbide (SiC) and palm kernel shell ash (PKSA) particulates at different weight ratios ranging from 0 to 10 wt. % with 2 wt.% intervals were investigated. The liquid route of double stir casting was employed in synthesizing the composites. The wear experiment was conducted using the Taber-type wear abrasion machine. The worn surfaces were examined using scanning electron microscopy (SEM) with energy-dispersive x-ray spectroscopy (EDS), while the intermetallic phases were examined using the x-ray diffractometer (XRD). From the result, the increase in PKSA and SiC lowered and improved the density of the composites, respectively. The percentage porosity values (2 - 2.4%) obtained in this study were found to be within the acceptable limit of less than 4% for metal matrix composites castings. The mass loss and wear index increased owing to the rotating speed and applied load increase due to the occurrence of mechanical mixing between the contacting surface of the sample disk and the machined disc. Adhesive and abrasive wear mechanisms were the major mechanisms observed in this study. The produced sample showed low wear resistance and will be found useful in areas with low frictional interactions.

Keywords: Mechanical properties; silicon carbide; palm kernel shell ash; Aluminium matrix composite; wear mechanism

INTRODUCTION

Recently, the development in the synthesis of metal matrix composites (MMCs) as advanced engineering materials has been the focus of many studies [1–5]; because of the application of MMCs in different engineering industries. Some of these industries where MMCs have found usages are in electrical cable, automobile engine and parts, oil and gas, aerospace, marine, sports, and many more. They have better properties, including high elastic modulus, high strength, and low density compared to metal alloys; hence, they are seen to be indispensable materials [6–8].

The production of various automobile parts (valves, pistons, and so on) with the utilization of MMCs have been implemented by some automobile industries (Honda, Nissan, and General Motors) all over the world [7]. The production of MMCs involves the usage of different metal matrices such as aluminium, magnesium, and so on. However, aluminium alloy is the most generally utilized matrix of all the alloys. Aluminium alloys have various categories and have good properties which include their lightweight, good electrical, and thermal electrical conductivities, and are highly resistant to corrosion [6,9].

The synthesis of MMCs requires the introduction of reinforcement particulates into the matrix. The introduced reinforcement particulates are categorized into ceramic/synthetic reinforcements (SiC, Al_2O_3, B_4C, TiC) and agro/industrial wastes ash (coconut husk ash (CSA), bean pod ash (BPA), rice husk ash (RHA), and so on) [1,10]. The ceramic reinforcements are hard in nature and their production is expensive. However, agro/industrial wastes ashes are easily obtained and cheaply processed for usage in MMCs production. These two categories of reinforcement can be used as single reinforcement or hybrid reinforcements. Single reinforcement is the usage of a single ceramic reinforcement or agro/industrial wastes ash in a matrix, which is normally termed "monolithic reinforcement", while hybrid reinforcements could be such that there will be a combination of two or more ceramic particulates, two or more agro/industrial waste ash particulates, or two or more ceramic and agro/industrial wastes ash particulates [1–3,10,11]. The inclusion of these reinforcing particulates into the matrix alloy is for the enhancement of the properties of the MMCs produced [12,13].

Recently, the usage of these agro/industrial wastes ashes as reinforcements in MMCs production either as monolithic or hybrid reinforcements has been the focus of many researchers. The type of reinforcements used has various effects on the tribological performance of the composite produced, where the final properties are functions of the used reinforcements characteristics [14]. Stir casting, squeeze casting, powder metallurgy, high-ball milling, compo-casting, and many more are the different methods that have been utilized in different studies for MMCs fabrication. However, the most economical method is stir casting [7,15,16]. This is owing to its cheapness, better materials yield, ability to produce intricate shapes with fewer damages [7].

One of the constantly experienced challenges in engineering industries is the disintegration of machine parts (known as wear) due to the rubbing action of the mating parts which is repeatedly slow and progressive. Wear happens due to the

speed of movement of the parts against each other, conditions of the environment, as well as the working load. Many industries spend enormous money to repair and replace worn-out parts. This is the bane behind the investigation of the wear properties of synthesized MMCs, to determine the areas that they will be found applicable. The wear resistance of MMCs is a function of the size of the particle, distribution of the reinforcement, shape, and volume fraction [8,9].

The tribological behaviour of different synthesized MMCs with monolithic or hybrid reinforcement particulates has been studied. Under a dry condition, the effects of load on the wear and worn surface friction were investigated using a pin-on-disc type apparatus [9]. The reinforcement particulate used was TiC and its variation in the AA7075 matrix was between 2 and 10 wt.%. In the study, a higher rate of wear and lower coefficient of friction (COF) for the matrix and composites were as a result of higher load applied. Both the mechanical and tribological properties of AMCs produced via the technique of powder metallurgy were investigated by Halil et al. [6]. The matrix used was Al6061, while the hybrid ceramic reinforcements of SiC and B_4C particulates were used for the production of the Al MMCs. The declination of the COF and the wear rate is attributed to the increased applied load and sliding distance, respectively.

The liquid metallurgy route was used to produce composites using LM13 alloy and garnet reinforcement with a different range of sizes. Wear experiments were done by varying the applied loads (9.8 – 49 N), while the sliding speed (1.6 m/s) and distance (3000 m) were made constant. The wear behaviour of the composites was influenced by the variation of the garnet mineral particle size. Coarse size garnet particulates showed a high wear rate at all loads compared to fine size garnet mineral particulates. The general structures detected on the worn surface show abrasion, adhesion, adhesion joints, and the formation of cracks [17]. Prasad and Shoba [18] examined the dry sliding tribological characteristics of AMCs synthesized using aluminium (Al) as the matrix, while RHA and SiC were used as the hybrid reinforcements in the composites up to 8% (in equal proportions). The technique of production was through the vortex method. The wear experiment for both the unreinforced and hybrid reinforced composites was done using the Pin-on disk wear test. It was revealed that higher wear resistance was seen in the hybrid composites compared to the unreinforced alloy. The wear resistance increment was credited to the matrix strengthening mechanism caused by the thermal mismatch between the reinforcing particulates and the matrix. The mechanisms of wear reported in the study were adhesive and abrasive wear mechanisms. Kumar and Birru [12] utilized single reinforcement of bamboo leaf ash (BLA) in the Al matrix and examined the wear properties of MMCs synthesized. The wear experiment was done utilizing pin-on-disc wear test apparatus. The wear rate reduces with an increase in BLA content. The analyzed wear mechanism via SEM-EDS revealed reduction in groove sizes as BLA particulates increase in the matrix. The AMCs wear resistance was observed to be significantly improved due to the formation of mechanical mixed layer on the composites.

In a study conducted by Alaneme et al. [15], the wear rate trend has no definite pattern. Nevertheless, a high rate of wear was observed for high alumina content composites compared to the low ones. Furthermore, the hybrid particulates of Al_2O_3, graphite, and rice husk ash (RHA) were utilized for the production of AMCs by Alaneme and Sanusi [16]. Noteworthily, composites with no graphite addition showed superior wear susceptibility unlike the composites with graphite. However, the increase in graphite contents reduced the rate of wear of the composites. The effect of the RHA particulates in the matrix on the wear susceptibility has no consistent trend. Although, the relationship between the wear susceptibility and the RHA contents increases proportionally. Ponugoti et al. [13] characterized the wear properties of synthesized Al6061/9% Gr/WC hybrid MMCs. The wear properties and COF were determined through variation of the percentage of the reinforcing particulates, sliding distance, applied load, and sliding velocity. Among several studies that have been done on MMCs' wear behaviour and optimization were Reddy et al. [7], Madhavarao et al. [19], Dharanikota [20], Dharmalingam et al. [21], Veličković et al. [14], and so on.

The tribological behaviour of the Al6063 matrix reinforced with SiC and palm kernel shell ash (PKSA) has not been fully investigated. The optimization of the wear behaviour of hybrid reinforced Al6063 with PKSA and SiC has been previously investigated by Ikubanni et al. [22] and the preliminary study on the tribological characteristics of the composites has been presented in Ikubanni et al. [23]. This study is an expanded investigation of the study of Ikubanni et al. [23]. The physico-tribological properties of Al6063/SiC/PKSA were examined and the different wear mechanisms occurrence in the composites are studied using scanning electron microscopy (SEM) equipped with energy dispersive spectroscopy (EDS).

MATERIAL AND METHODS

The base matrix used in this study for the production of the composites is an Al6063 alloy billet with the chemical composition given in wt.% as Si (0.43), Fe (0.17), Mn (0.04), Mg (0.48), Cu (0.01), Ti (0.02), Zn (0.01), Cr (0.01), Sn (0.01), and the balance is aluminium. With the matrix, the composite was produced using hybrid reinforcement of PKSA and SiC particulates. The palm kernel shell (PKS) obtained in a local area in Osun State was processed by sorting, cleaning, drying, and subjecting the PKS to a temperature of 900ºC for 4 h to produce PKSA. The particulate size of the PKSA used was sieved below 40 μm, and SiC of 30 μm average particle size was used. **Table 1** displays the chemical oxides present in the PKSA in wt.%.

Table 1 PKSA Chemical composition (%)

Chemical composition	Na_2O	MgO	Al_2O_3	SiO_2	P_2O_5	K_2O	CaO	TiO_2	Fe_2O_3	MnO	LOI
%	0.17	3.14	6.46	66.90	3.78	5.20	5.52	0.53	5.72	0.08	2.50

Hybrid composite synthesis

Double stir casting was utilized in developing the composites in this study, which is a popular liquid metallurgy route. This technique has been used by many researchers and has been adjudged to produce good castings [15,22]. Based on the different mix proportions of the Al6063, SiC, and PKSA as presented in **Table 2** for which the reinforcement particulates were to be between 0 and 10 wt.%, the charge calculation was carried out to evaluate the amounts of materials to be used. For the moisture content of the reinforcement particulates to be reduced and also for their wettability to be improved with the base metal, PKSA and SiC reinforcement particulates were preheated at a temperature of 250℃ [16]. The matrix (Al6063 alloy) billets were charged into a gas-fired crucible furnace, which was then fired up to a temperature of 750°C ± 30°C. At a temperature of about 600ºC, the molten matrix was made to

cool in the furnace to a semi-solid state. Then, the reinforcement particulates which were initially preheated were poured into the semi-solid state matrix alloy. The molten matrix and reinforcements form slurry, which was stirred manually for close to 10 minutes. The manually stirred semi-solid composition in the furnace was superheated to about 780°C ± 30°C temperature. A second stirring for the composite was done mechanically at a mean rotating speed of 400 rpm for 10 minutes. The second mechanical stirring process is to assist in the uniform reinforcement particulate distribution in the semi-solid matrix by disintegrating particulate accumulation at a spot. Thereafter, the semi-solid composites were discharged into prepared sand mould for solidification. **Fig. 1** displays the solidified wear sample produced.

Fig.1 Samples produced for wear experiment

Table 2 Composite designation

Al6063/PKSA/SiC (wt.%)	Sample designation
100/0/0	CA
98/0/2	CB
96/2/2	CC
94/4/2	CD
92/6/2	CE
90/8/2	CF
98/2/0	CG
94/2/4	CH
92/2/6	CI
90/2/8	CJ

Density and porosity determination

The impact of the variation of the hybrid reinforcements (PKSA and SiC) on the density of each of the composites produced was investigated by obtaining the experimental and theoretical densities. The theoretical density was obtained through the rules of mixtures of the constituent materials for the production of the composites. However, the mass and volume of each produced composites were measured and the ratio of the mass and volume gave the value of the experimental density for each composition. Equation (1) was employed to estimate the percentage porosity of the composites.

$$\%Porosity = \frac{\rho_T - \rho_{Ex}}{\rho_T} \times 100\% \quad (1.)$$

Where ρ_T, ρ_{Ex} are theoretical density and experimental density (in g/cm^3), respectively.

Tribological characteristics

For wear resistance determination of the composites, this study utilized the TSE-A016 model Taber Type Abrasion tester following the ASTM D4060-16 standard. **Fig. 2** showed machined test samples with dimensions, thickness (5 mm), and diameter (100 mm). For the wear experiment, the surface of the composite specimen was positioned on the Taber abrasion machine's turntable platform gripped by two abrasive wheels lowered at constant pressure on the sample's surface. Four different applied loads (250, 500, 750, and 1000 g) and rotating speeds (250, 500, 50, and 1000 rpm) were utilized on each sample. There is a generation of debris as a result of sample-abrasive wheels rubbing action. Therefore, the weight before and weight after the experiment were measured after 15 minutes duration of the experimentation.

The composites' tribological properties were then obtained using Eqs. (2-3). Equations 2 (a) and (b) were utilized to evaluate the mass loss (g) and volume loss (mm^3), respectively.

$$Mass\ loss = Initial\ mass\ (m_i) - Final\ mass\ (m_f) \quad (2a.)$$

$$Volume\ loss = \frac{mass\ loss}{\rho} \quad (2b.)$$

Equation (3) was utilized to determine the Taber wear rate index

$$Taber\ Wear\ Index, I = \frac{m_i - m_f}{T} \times 1000 \quad (3.)$$

Where ρ = Composite density, T = time of test cycles (min), and I = Taber wear index.

Fig. 2 Wear sample

SEM and XRD analysis

The phases present in the developed composites were obtained using a PANalytical Empyrean diffractometer (X-ray diffractometer). Its specifications include with 40 mA current, 45 kV acceleration voltage, 1.5406Å Cu K_α radiation, and a 5 – 90^o scan range (2θ) with 0.026^o/min scan speed. To the diffractometer, there was an attachment of X'Pert Highscore Plus software for picking mineral phases.

The structural morphologies of the synthesized composites were obtained with a Vega 3 TESCAN model SEM with EDS attachment. Before performing the microscopic investigation, polishing and etching of the samples were metallographically performed and then positioned in the SEM equipment. The image of the samples with the SEM, while the elemental compositions were obtained using the EDS attachment. More so, the worn-out surfaces were examined using the SEM-EDS equipment.

RESULTS AND DISCUSSION

Influence of the hybrid reinforcements on the physical properties

Fig. 3 displays both the value of the experimental density, as well as the porosity value for composites, developed. The unreinforced alloy's (Sample CA) experimental density was 2.64 g/cm^3 and 2.063% percentage porosity. The sample composition with the highest density is Sample CB with a value of 2.65 g/cm^3. In this sample, 98% CB and 2% SiC are used in developing the composite. The high density of this sample might be due to the hardness of the SiC reinforcement addition into the matrix alloy. It is observed that there is a

gradual decline in the density values of samples CC – CF. The gradual declination of these density values could be credited to the weight percentage reduction in the Al percentage and increasing the weight percentage of light-weight PKSA while the weight percentage of SiC was left constant at 2% for the samples CC – CF. Hence, the low density of PKSA in comparison to SiC and Al resulted in the reduction of the density as the PKSA value increases with a decrease in CB quantity. This study is in concordance with the observation of Prasad et al. [24]. Noteworthy, there was a noticeable increase in the density of sample CG, which resulted from the quantity of Al (98 wt.%) and PKSA (2 wt.%) present in the designated composition. The lower the amount of PKSA present in a composition with a higher CB content, the better the density whether theoretically or experimentally. The increase of sample CG density compared to the density of samples CD - CF could be credited to the increased Al matrix alloy quantity and decreased PKSA particulates in the composites. The density of samples CH – CJ gradually improved as seen in **Fig. 3.** This improved density could be ascribed to the increased wt.% SiC in the composition with a constant PKSA percentage weight of 2 %, while the quantity of Al matrix is the balance. The hard nature of SiC was responsible for the increment in the density of the composites.

The porosity percentage values of the samples were less than 2.5% in which the maximum acceptable limit (< 4%) was reported for cast MMCs [16]. Therefore, the liquid metallurgy route employed for the composite development is said to be reliable and efficient because the technique breaks surface tensions between the particulates and the matrix alloy, which permits aspirated air-bubble entrapped into the slurry escape during the processing [15].

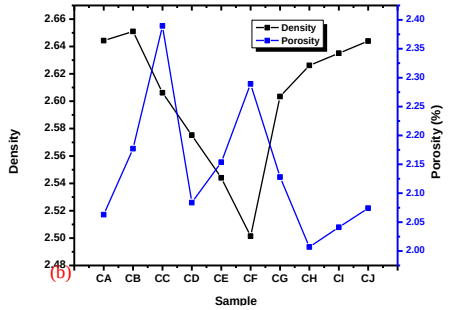

Fig. 3 Developed percentage porosity and experimental density of the composites

Morphology and structural characterization of the unreinforced and reinforced composites

The surface of the unreinforced and reinforced alloys was subjected to morphological examination using SEM. The representative microstructures of the unreinforced and reinforced MMCs developed were displayed in **Fig. 4**. Visible and uniformly dispersed reinforcement particulates are observed in the Al6063 alloy matrix. In the micrographs, there are hardly noticeable particulate clusters. Based on the level of dispersion of the reinforcing particulates in the alloy metal, the method of casting utilized is adjudged to be very good and acceptable. Hence, since there is no particulate distribution inhomogeneity, there is no likelihood for induced anisotropy [15]. The interfacial nucleation sites formation increases within the composites due to increment in PKSA particulates weight fraction. There is a very high tendency for the inhibition of alpha-Al grains devolvement in the matrix alloy due to the distribution of the PKSA particles. The more the PKSA content in the composites, the higher is the formation of the grain nucleation sites, which could permit the free development of alpha-Al grains that produces grain refinement [25, 26]. This grain refinement could result in obtaining better mechanical properties such as hardness, yield strength, and ultimate tensile strength for the composites developed. Hence, a grain size decrement improves the strength of composites [25].

The EDS spectrum for Fig. 4 (a) as shown in **Fig. 5** (a) displays aluminium (Al), silicon (Si), magnesium (Mg), and iron (Fe) peaks. This was in line with the elemental compositions of the matrix alloy used for the composite production. The major alloying elements in Al6063 are Si, Mg, and Fe. Other elements are seen as trace elements. Figure 5(b) is the EDS spectrum for **Fig. 4(b)**, which displays aluminium (Al), silicon (Si), magnesium (Mg), iron (Fe), and oxygen (O) the peaks. The existence of these elements affirms the presence of the various oxides of the elements such as silica (SiO_2), alumina (Al_2O_3), ferric oxide (Fe_2O_3), and magnesium oxide (MgO).

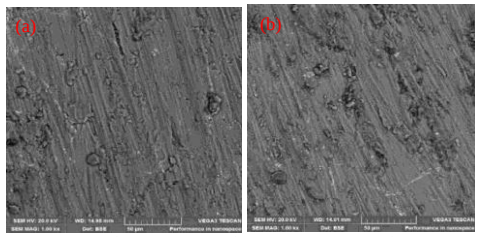

Fig. 4 SEM of the (a) unreinforced alloy (b) reinforced alloy with 2 wt.% PKSA and 4 wt.% SiC

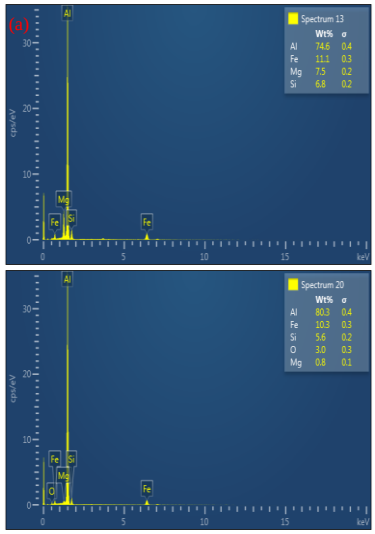

Fig. 5 EDS of the (a) unreinforced alloy (b) reinforced alloy with 2 wt.% PKSA and 4 wt.% SiC

The XRD spectra for the composites synthesized are displayed in **Fig. 6**. It can be observed that in the unreinforced alloy, cubic crystal system aluminium was detected by the machine used. The reason for none detection of other phases might be due to the low weight percentage of other elemental constituents in the unreinforced alloy (**Fig. 6a**). Noteworthily, there are different peaks of the phases present that was detected in the reinforced alloy. Aside from the Al peak, intermetallic

cubic crystal system phase of Fe_3Si peak, MgO, SiO_2, and SiC peaks were also present. The Fe_3Si, MgO, SiO_2, and SiC peaks are seen to be minor peaks. This is a reflection of the small amount of intermetallics present. Summarily, the composition of the reinforcing particulates influenced the compound detected as well as the phase intensities [15].

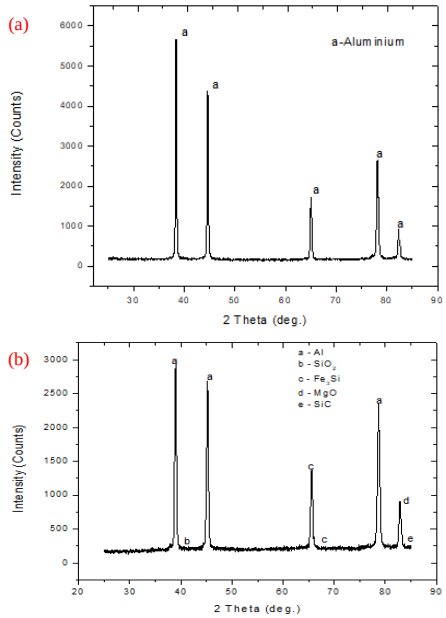

Fig. 6 XRD of the (a) unreinforced alloy (b) reinforced alloy with 2 wt.% PKSA and 4 wt.% SiC

Variation effects of sliding speed and applied load on mass loss

The disparity of the mass loss with the different sample compositions when subjected to four different loads and speeds, respectively are shown in **Figs. 7 – 10**. It was noticed that more amounts of materials are lost as the rotational speed increases, showing a direct proportionality between the worn mass and sliding speed. In addition, the applied load value influences the rate of material removal – increasing the load will cause more volume of material removed from the sample (**Figs. 7 – 10**). The load increment could have resulted in the generation of more heat due to increased friction between the rotating wheels and the composites, which would increase the material loss as well as wear of the composite. In essence, friction caused heat generation between the rotating wheel and the surface of the composite samples amounts to an increased localized surface temperature that softens the surface of the samples. As shear forces exist between the two surfaces, material removal occurs on the softer surface, resulting to wear of the composite samples [18,27]. The rough layers on the surface of the samples could be ascribed to the initial contact time, which consequentially produced smoothened and clean surfaces. Hence, the interaction of the composite sample surface with the rotating wheel increased the contact strength. There is increased material loss deposited on the surface of the samples. These worn particles may smear onto the surface of the rotating wheel by adhesion to form asperities, increasing the pull-off action by the rotating wheel on the sample surface. Hence, abrasive wear occurs at the surface of the composite samples [28]. There is no consistent pattern in the mass loss of the composites due to the inclusion of the hybrid reinforcements. However, samples CH and CI showed better wear resistance for all the samples based on the values obtained for all the applied loads. This could be attributed to the reinforcement particulate accumulation that is squeezed on the surface through the deformation of the subsurface, which transforms into lubricating film or tribo-layer formation.

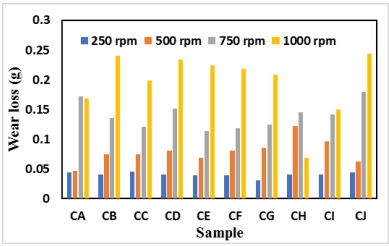

Fig. 7 Mass loss at 250 g load

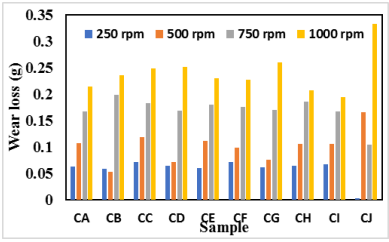

Fig. 8 Mass loss at 500 g load

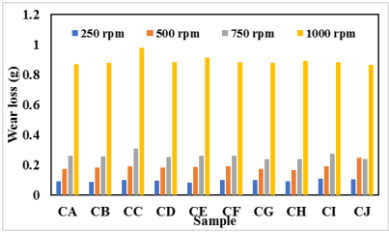

Fig. 9 Mass loss 750 g load

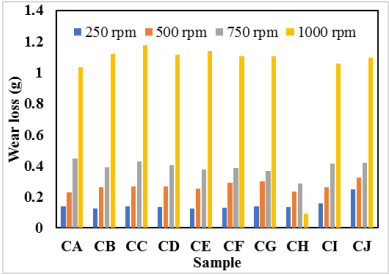

Fig. 10 Mass loss at 1000 g load

Wear index and sliding speed influence

At different applied loads and speeds, **Figs. 11 – 14** display the wear indices of the composite samples. It is noticeable that there is a proportional variation between the wear index and sliding speed. At different loads, the lower the sliding speed, the smaller the wear index obtained, and the sliding speed

increases, more wear index is obtained. More so, the wear index rises with an increase in the load applied. This finding agrees with the study of Adediran et al. [28], which reported increased wear rate and volume loss with increased applied load.

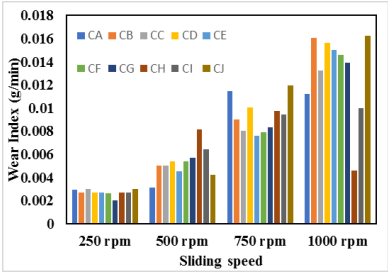

Fig. 11 Wear index against sliding speed at 250 g load

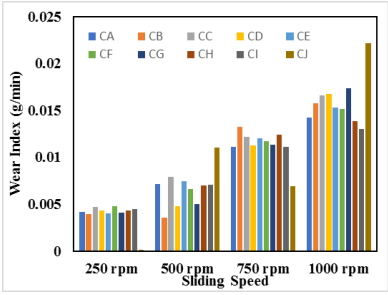

Fig. 12 Wear index against sliding speed at 500 g load

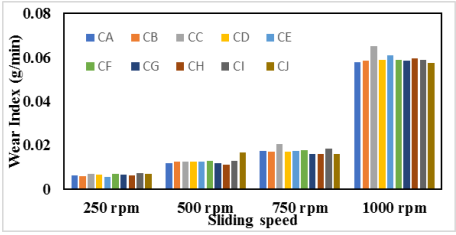

Fig. 13 Wear index against sliding speed at 750 g load

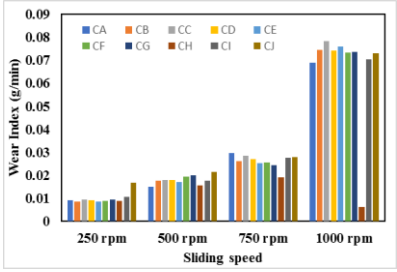

Fig. 14 Wear index against sliding speed at 1000 g load

Wear morphology and mechanism

The worn surfaces of all the sample compositions were analyzed using SEM. This is to discover the wear mechanisms. Wear conditions are reported to affect the wear mechanisms. The mechanisms occurring in Al MMCs are abrasive, adhesion, delamination, and abrasion wear [6]. The worn surfaces reveal abrasion wear (**Fig. 15 (a-j)**). Wear cracks were also seen on the worn surfaces, for instance, in **Fig. 15 (a, c d, g, and i)**. In addition, there is a great parallel alignment between the sliding direction and the grooves created. **Figure 15(a)** reveals the SEM images of the unreinforced alloy's worn-out surface. It reveals grooves and ridges that are running parallel to the sliding direction. This is an indication of abrasive wear and adhesive wear (crater). This is in line with the observations of Prasad and Shoba [18]. It is important to state that the occurrence of abrasive wear is a result of hard asperities or particles that rub under load against a relatively softer surface [29]. It was observed that the dominant wear mechanism in the unreinforced alloy is abrasive wear. The grooves formation on the substrate is a result of the ploughing action of the hard contact surface.

Some of the micrographs reveal a large cavity on the subsurface layer, which indicates a severe material loss. However, it was observed that as the load increases, the large cavity became significant. **Figure 15 (b)** reveals the SEM morphology of the worn-out surface of the sample with Al matrix reinforced with 2 wt.% SiC. The SiC particulates displayed good bonding, which cannot be pulled out from the matrix. The SiC, which is a hard material, could be responsible for the increased resistance to wear [6]. It is worthy of note that the presence of grooves reveals the effect of micro-ploughing and micro-cutting. **Figure 15 (c)** shows the morphology of the worn-out surface of the sample CC (Al6063/2 wt.% SiC/2 wt.% PKSA). It can be seen that there is a material plastic flow and with some smooth patches and ridges, which run in parallel to the sliding direction. Some portions of the SEM morphology of the worn-out surface show areas that have larger craters, cavities, and delamination. These are also observed in the SEM images of the other compositions (**Fig. 15 (d) – (j)**). Delaminated areas in the SEM are known to be delamination wear mechanisms, which are usually due to deformation and material removal. The cavity presence can be attributed to deformation that occurs due to work-hardening of the matrix. Work-hardening is increased when working with higher loads, which could result in cracks in the interfaces of the matrix and reinforcement. The propagation of cracks can further be interlinked to cause deformation and delamination of the matrix alloy. Hence, delamination wear is the end product of the cracks. Larger cavities (deformation areas) are seen in the SEM images (**Fig. 15**). Furthermore, higher loads cause pull-out of particles that result in void formation, which are centres for crack initiation [17]. Although, intact particles form resistance to the growth of the crack. There is a formation of subsurface delamination through the wear cracks coalescence at higher applied load. On the worn-out surface, the different localized delamination areas are joined to form larger craters. More so, from the worn surface, there is mechanical mixed layer (MML) formation due to the fine size debris that adheres within the cavity formed by the delaminated layer [12, 17]. The rise in temperature as a result of heat generated by friction facilitates the formation of the oxide of Al through oxidation. The oxide formation on the worn surfaces of the composites is confirmed based on the EDS spectra 5 and 6 (**Fig. 16 (b) and (c)**), which reveal Al, Mg, Si, Fe, and O peaks in the selected zones. The iron (Fe) and oxygen (O) presence in the spectra supports oxide layer formation during the wear experiment. This is an indication of the occurrence of the mechanical mixing between the Taber wear disc and the wear sample, which is more noticeable at higher loads than at lower loads [14, 18, 30]. Different wear mechanisms are seen to occur on the surfaces of the worn samples. The general structures discovered on the worn-out surfaces exhibit abrasion, adhesion,

and formation of cracks and cavities. The study of Halil et al. [6] showed a similar trend of wear mechanism when single and hybrid reinforcement of SiC and B_4C were used as reinforcements in Al6061 matrix.

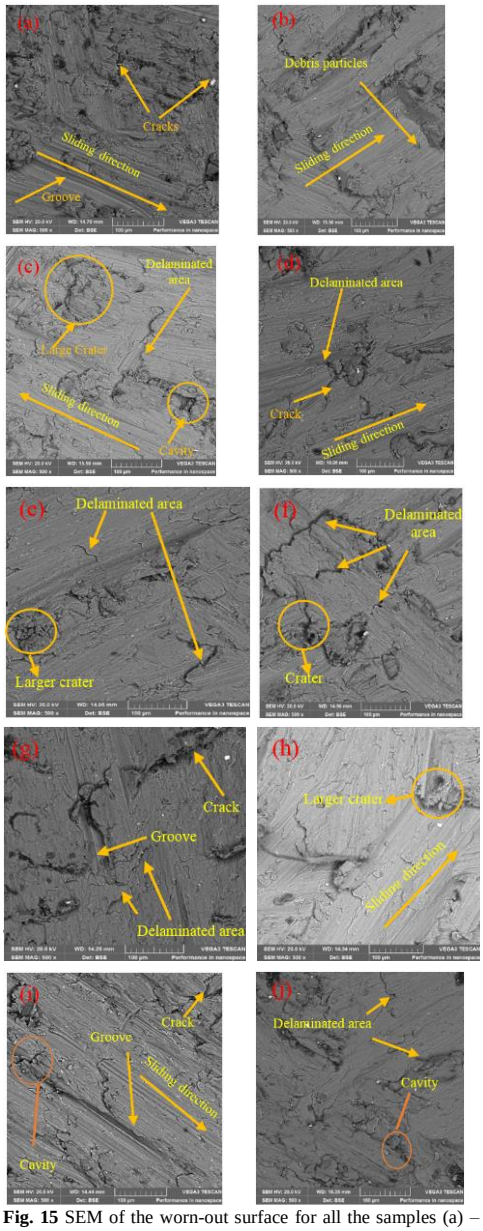

Fig. 15 SEM of the worn-out surface for all the samples (a) – (j) (Sample CA – sample CJ), respectively

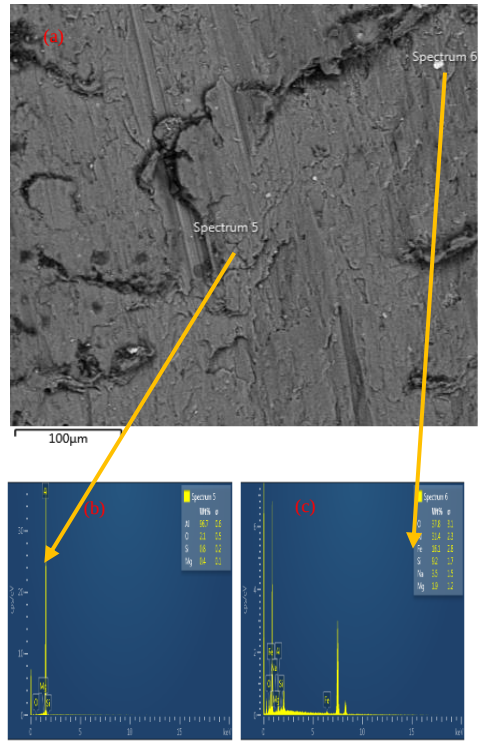

Fig. 16 Representative sample (a) SEM, and EDS of (b) spectrum 5 (c) Spectrum 6

CONCLUSION

In this study, the physico-tribological characteristics of AMCs synthesized using hybrid reinforcing particulates of PKSA and SiC were considered. The density obtained showed reduction as the PKSA particulates increase when SiC was made constant at 2 wt.% in samples CC – CF. However, there was a density increment when PKSA was made constant (2 wt.%) with SiC contents variation in samples CH – CJ, which was lower than the unreinforced alloy. The reinforcements were uniformly dispersed in the matrix alloy and phases such as Fe_3Si, MgO, SiO_2, and SiC peaks were identified. The increase in speed and applied load increases the mass loss as well as the Taber wear index. The wear index of the composite is high. The micrographs showed that the wear mechanisms in this present study were majorly adhesive and abrasive. There is the formation of the oxide of Al via oxidation due to frictional heat generation resulting in temperature rise, which was confirmed from the EDS spectra. The oxide layer formation was supported by the presence of iron (Fe) and oxygen (O) in the spectra. This is an occurrence of the mechanical mixing between the Taber wear disc and the counter-face disk indicating the greater loss of materials as load increases. The produced sample showed low wear resistance and will be found useful in areas with low frictional interactions.

REFERENCES

1. P.P. Ikubanni, M. Oki, A.A. Adeleke: Cogent Engineering, 7, 2020, 1–19. https://doi.org/10.1080/23311916.2020.1727167.
2. P.P. Ikubanni, M. Oki, A.A. Adeleke, A.A. Adediran, O.S. Adesina: Results in Engineering, 8, 2020, 1-9.

https://doi.org/10.1016/j.rineng.2020.100173
3. M.O. Bodunrin, K.K. Alaneme, L.H. Chown: Journal of Material Research and Technology, 4, 2015, 434–445. https://doi.org/10.1016/j.jmrt.2015.05.003.
4. S.T. Mavhungu, E.T. Akinlabi, M.A. Onitiri, F.M. Varachia, Aluminum Matrix Composites for Industrial Use: Advances and Trends, in: *Int. Conf. Sustain. Mater. Process. Manuf. SMPM 2017*, 23-35 January 2017, Kruger Natl. Park Publ. Procedia Manuf., Procedia Manufacturing, Elsevier, South Africa, 2017: pp. 178–182. https://doi.org/10.1016/j.promfg.2016.12.045.
5. U.R. Kanth, P.Rao, M.G. Krishna: Journal of Material Research and Technology, 8, 2019, 737–744. https://doi.org/10.1016/j.jmrt.2018.06.003.
6. K. Halil, O. Ismail, D. Sibel, Ç. Ramazan: Journal of Material Research and Technology, 8, 2019, 5348–5361. https://doi.org/10.1016/j.jmrt.2019.09.002.
7. P.V. Reddy, P.R. Prasad, D.M. Krishnudu, E.V. Goud: Journal of Bio- and Tribo-Corrosion, 5, 2019, 1–10. https://doi.org/10.1007/s40735-019-0282-0.
8. L.F. Xavier, P. Suresh: Scientific World Journal, 2016, 2016, 1–8. https://doi.org/10.1155/2016/6538345.
9. V.R. Rao, N. Ramanaiah, M.M.M. Sarcar: International Journal of Applied Science and Engineering, 14, 2016, 27–37.
10. T.A. Orhadahwe, O.O. Ajide, A.A. Adeleke, P.P. Ikubanni: Arab Journal of Basic and Applied Science. 27, 2020. https://doi.org/10.1080/25765299.2020.1830529.
11. M.B.A. Shuvho, M.A. Chowdhury, M. Kchaou, B.K. Roy, A. Rahman, M.A. Islam: Chemical Data Collection, 28, 2020. https://doi.org/10.1016/j.cdc.2020.100442.
12. B.P. Kumar, A.K. Birru: Tribology in Industry, 40, 2018, 311–325. https://doi.org/10.24874/ti.2018.40.02.14.
13. G.R. Ponugoti, P.R. Vundavilli, A.G. Krishna, Optimization of tribological properties of Al6061/9% Gr/WC hybrid metal matrix composites using FGRA, in: Adv. Manuf. Technol. ICAMT 2018, Springer Singapore, 2019: pp. 485–492. https://doi.org/10.1007/978-981-13-6374-0.
14. S. Veličković, B. Stojanović, M. Babić, I. Bobić: Journal of Composite Materials, 51, 2017, 2505–2515. https://doi.org/10.1177/0021998316672294.
15. K.K. Alaneme, M.H. Adegun, A.G. Archibong, E.A. Okotete: Journal of Chemical Technology and Metallurgy, 54, 2019, 1361-1370.
16. K.K. Alaneme, O.K. Sanusi: Engineering Science and Technology- an International Journal, 18, 2015, 416–422. https://doi.org/10.1016/j.jestch.2015.02.003.
17. S. Kumar, A. Sharma, R. Arora, O.P. Pandey: Journal of Material Research and Technology, 8, 2019, 5443–5455. https://doi.org/10.1016/j.jmrt.2019.09.012.
18. D.S. Prasad, C. Shoba: Journal of Material Research and Technology, 3, 2014, 172–178.
19. S. Madhavarao, C.H. Raju, J. Madhukiran, N.S. Varma, P.R. Varma: Material Today Proceedings, 5, 2018, 20013–20022. https://doi.org/10.1016/j.matpr.2018.06.368.
20. V. Dharanikota: International Journal of Science and Engineering Research, 5, 2014, 629–637.
21. S. Dharmalingam, R. Subramanian, K.S. Vinoth, B. Anandavel: Journal of Material Engineering and Performance, 20, 2011, 1457–1466. https://doi.org/10.1007/s11665-010-9800-4.
22. P.P. Ikubanni, M. Oki, A.A. Adeleke, O.O. Agboola: Scientific African, 12, 2021. https://doi.org/doi.org/10.1016/j.sciaf.2021.e00839.
23. P.P. Ikubanni, M. Oki, A.A. Adeleke, A.A. Adediran, O.O. Agboola, O. Babayeju, N. Egbo, I.M.B. Omiogbemi: Material Today Proceedings, 2021. https://doi.org/10.1016/j.matpr.2021.03.537.
24. D.V. Prasad, C. Shoba, N. Ramanaiah: Journal of Material Research and Technology, 3, 2014, 79–85.
25. P.K. Bannaravuri, A.K. Birru: Results in Physics, 10, 2018, 360–373. https://doi.org/10.1016/j.rinp.2018.06.004.
26. B.P. Kumar, A.K. Birru: Transaction of the Nonferrous Metal Society of China, 27, 2017, 2555–2572. https://doi.org/10.1016/S1003-6326(17)60284-X.
27. R. Al-Samarai, Haftirman, K. Ahmad, Y. Al-Douri: International Journal of Scientific and Research Publications, 2,(2012, 1–4. https://doi.org/10.4236/jsemat.2012.23027.
28. A.A. Adediran, K.K. Alaneme, I.O. Oladele, E.T. Akinlabi: Cogent Engineering, 7, 2020, 1–19. https://doi.org/10.1080/23311916.2020.1826634.
29. K.K. Alaneme, A.V. Fajemisin, N.B. Maledi: Journal of Material Research and Technology, 8, 2019, 670–682. https://doi.org/https://doi.org/10.1016/j.jmrt.2018.04.019.
30. G.B.V. Kumar, P. Prasad, N. Suresh, R. Pramod, C.S.P. Rao: Composites Part B, 175, 2019, 107138. https://doi.org/10.1016/j.compositesb.2019.107138.